Journal of Materials Chemistry A

Accepted Manuscript

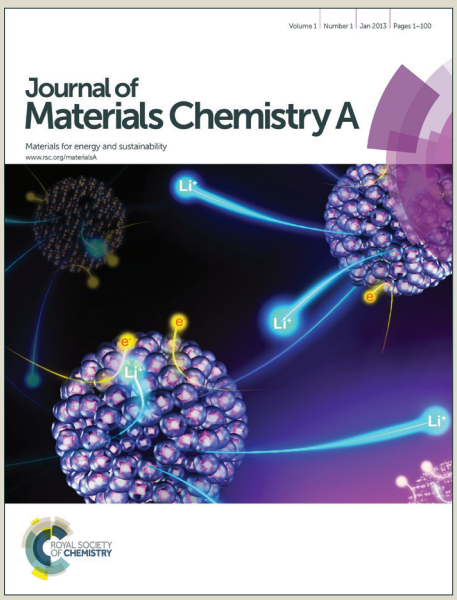

ROYAL SOCIETY OF CHEMISTRY

www.rsc.org/materialsA

The table of contents entry

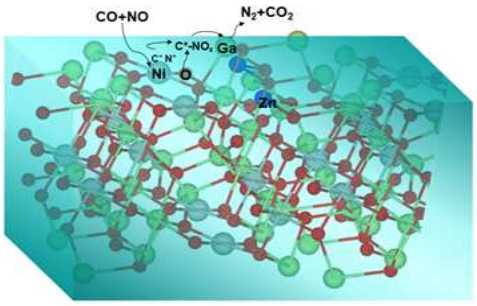

C*: carbon-containing active species
N*: nitrogen-containing active species

As a typical example of bifunctional catalyst, a new low-cost Ni-Ga based oxide catalyst with inverse spinel structure was developed for NO removal, which exhibits the synergetic catalysis of Ni and Ga: strong NO capture from Ni species and applicable NO catalytic conversion from both Ni and Ga species. Our results open a new route to design the efficient catalysts combining the strong gas capture by specific elements and the high catalytic NO conversion by constructing appropriate elements ligand environment.

Keyword: NO_x removal, bifunctional catalyst, Ni-Ga based compound

Shicheng Yan,* Zhaochun Wu, Qian Xu, Jia Jia Wang, Jinhua Hong, Jixue Li, Peng Wang, Zhigang Zou

Title: Catalytically converting the NO_x by difunctional Ni-Ga based oxide catalyst

Catalytic reduction of NOx by CO over Ni-Ga based oxide catalyst

Shicheng Yan[a,b], Zhaochun Wu[c], Qian Xu[a], Jia Jia Wang[a,b], Jinhua Hong[d], Jixue Li[d], Peng Wang[a], Zhigang Zou[a,b,c]*

[a]Collaborative Innovation Center of Advanced Microstructures, College of Engineering and Applied Sciences, Nanjing University, NO. 22, Hankou Road, Nanjing, Jiangsu 210093, P.R.China
[b]Eco-Materials and Renewable Energy Research Center (ERERC), College of Engineering and Applied Sciences , Nanjing University, NO. 22, Hankou Road, Nanjing, Jiangsu 210093, P.R.China, E-mail: yscfei@nju.edu.cn
[c]National Laboratory of Solid State Microstructures, School of Physics, Nanjing University, NO. 22, Hankou Road, Nanjing, Jiangsu 210093, P.R.China
[d]Department of Materials Science and Engineering, Zhejiang University, No.38, Zheda Road, Hangzhou, Zhejiang 310027, P. R. China.

Keywords: NO_x removal, bifunctional catalyst, Ni-Ga based compound

Abstract: Removal of nitrogen oxides (NO_x) originated from the human activities continues to be a challenge for environment protection due to lack of the efficient method to capture and convert the nitrogen oxides. Here, as a typical example of bifunctional catalyst, a new low-cost Ni-Ga based oxide catalyst with inverse spinel structure was developed for NO removal, which exhibits the synergetic catalysis of Ni and Ga: strong NO capture from Ni species and applicable NO catalytic conversion from both Ni and Ga species. The NO removal on Ni-Ga based catalyst is dependent strongly on Ga ligand environment. The largely inverse spinel with a inversion parameter of 92%, the tetrahedral preference of Ga^{3+}, greatly contribute to the high performance in NO conversion due to the electron transfer to occur easily in the low coordination environment of Ga ions. The electron transfer process in Ni-Ga based catalyst can be further activated by Zn doping, correspondingly increasing the catalytic ability in NO conversion. Our results open a new route to design the efficient catalysts combining the strong gas capture by specific elements and the high catalytic NO conversion by constructing appropriate elements ligand environment.

1. Introduction

Nitrogen oxides (NO_x), mostly nitric oxide (NO), are major pollutants in the atmosphere, being a precursor to acid rain, photochemical smog, and ozone accumulation. Since the industrial revolution, the NO_x content in the atmosphere increases largely due to the various human activities. Automobiles and other mobile sources contribute about half of the NO_x that is emitted. This brings the serial environment issues, which lead to a threat to survival of mankind and other life. The most widely adopted method to reduce NO_x emissions is catalytic reduction of NO_x to N_2 by reductants such as ammonia, CO and hydrocarbons.[1-3]

Generally, for the gas-phase conversion of NO, there are two processes: gas capture and gas conversion. The NO molecule is firstly captured on the surface of the catalyst by gas adsorption, and then is activated on the catalytic active sites to achieve the reduction process from NO to N_2. Therefore, the ideal catalyst must have strong gas adsorption for promoting the gas-phase reaction to proceed and be efficient in collecting and transporting charges for the chemical catalytic processes. A typical example is NO_x storage-reduction catalytic system, in which reaction NO_x is trapped by alkali metals such as Ba[4], K [5] and Na [6], and is reduced over noble metals such as Pt [7], Pd [8] and Rh [9]. Consequently, in principle, a NO_x storage-reduction catalyst should have sites for NO_x adsorption on the alkali or alkaline earth metals and sites for NO_x reduction on noble metals [10, 11]. The separate NO adsorption sites and catalytic conversion sites increased the complexity of the reaction and decreased the NO conversion efficiency. A promising route to overcome this obstacle is to combine the NO adsorption sites and catalytic conversion sites into a single compound. For example, a low-cost Ag/Al_2O_3 has been developed, which exhibited a strong catalytic ability in conversion of NO to NO_2 over Ag-related species. [12] In this article, the chief aim is developing the low-cost Ni-Ga based oxide catalysts with strong adsorbed ability and high catalytic activity for converting NO to N_2.

Gallium and nickel have *d* electronic configurations, which are active elements for catalytic reaction. In the present study, we use a new and nonprecious Ni-Ga oxide catalysts with inverse spniel structure for NO removal and show experimentally that it has the unique property that it converts NO to N_2 with high sensitivity in NO capture and catalytic conversion. The synergetic catalysis of Ni and Ga was achieved in a single oxide and resulted from the strong NO capture of Ni species and the high catalytic activity of the low coordination environment of Ga ions due to the electron transfer which occurs easily in the inverse spinel structure. The electron transfer process in Ni-Ga based inverse spinel catalyst can be further activated by Zn doping, significantly increasing the catalytic ability in NO conversion. An important consequence of the present investigation is to provide the new insight to developing the new strategies combining the strong NO capture by specific elements and the high catalytic ability by constructing appropriate element ligand environment for the removal of NO_x.

2. Experimental

Material preparation. To synthesize the $NaGaO_2$ powders, the 0.03mol of Na_2CO_3 and 0.03mol of Ga_2O_3 were mixed and ground in agate mortar for 30min. After that, the mixture of Na_2CO_3 and Ga_2O_3 was heated at 850 ^oC for 12h and furnace cooled to room temperature. The preparation procedure of $Ni_{1-x}Zn_xGa_2O_4$ ($0<x<1$) was performed as follows: the as-prepared $NaGaO_2$ powders (0.004mol) was dispersed in 25mL of deionized water and magnetically stirred for 10min to obtain the $NaGaO_2$ colloidal solution. The $NaGaO_2$ colloidal solution was added to 20mL of aqueous solution of $Zn(CH_3COO)_2{\cdot}2H_2O$ and $Ni(CH_3COO)_2{\cdot}4H_2O$ (Ni+Zn 0.004mol) and stirred for 30min at room temperature. The resulting mixture was heated in a 50mL of Teflon-lined hydrothermal autoclave at 200 °C for 5 h to form the crystalline $Ni_{1-x}Zn_xGa_2O_4$ ($0<x<1$). The sediment was separated by centrifugation and dried at 60 ^oC for 2h. Using the same hydrothermal procedure, the $ZnGa_2O_4$ and $NiGa_2O_4$ powders were prepared.

*Sample characterization.*The crystalline phases of these as-prepared products were determined by powder XRD. The as-prepared samples were placed on a zero background holder and transferred into a Rigaku Ultima III Diffractometer, which employs Cu Kα radiation at 40kV/40mA. Scans were run over the range of 10 to 80° with a step size of 0.01° and a counting time of 750 seconds per step. BET surface area measurements were conducted on a Micromeritics Tristar 3000 surface area and porosity analyzer. The sample, ~0.1 g, was placed in a tube and degassed for two hours at 300 ^{o}C. Multipoint BET measurements were conducted by nitrogen sorption at 77 K. The specific surface area calculated from the linear region of the BET plot ranging from P/P_0=0.05 to 0.15. The pore diameter calculated from the nitrogen adsorption isotherm by the Barrett-Joyner-Halenda (BJH) method. The morphologies, crystalline structure and local nanostructures of the $ZnGa_2O_4$, $NiGa_2O_4$ and $Ni_{0.9}Zn_{0.1}Ga_2O_4$ were observed by a field emission transmission electron microscope (TEM, FEI Tecnai G2 F30 S-Twin, USA). Atomic resolution high angle annular dark field (HAADF) images were acquired on a start-of-the-art FEI Titan ChemiSTEM 200kV with a probe aberration-corrector. The X-ray energy dispersive spectrum (EDS) mapping was carried out on the Titian using its Super-X detector technology. The electron paramagnetic resonance (EPR) spectra were obtained using a Bruker (model EMX-10/12 X-band) electron paramagnetic resonance spectrometer at the liquid nitrogen temperature of 77K. The settings were center field, 3480.0G; microwave frequency, 9.2-9.8GHz; power, 19.97mW.

Diffuse Reflectance Infrared Fourier Transform Spectroscopy (DRIFTS) accessory (Harrick's Praying Mantis) in conjunction with the FTIR (Thermo Nicolet 5700) at 4 cm^{-1} resolution was performed to identify NO wavenumbers for adsorption and oxidation reactions. The catalyst was first pretreated at 400 ^{o}C with high-purity Ar and then cooled down to 50 ^{o}C. The reaction chamber was flushed with Ar for 30 minutes to remove any residue and 50 scans were collected as the background. Thereafter, a controlled stream of CO-NO-Ar gas mixture (5% NO+10% CO+85% Ar by volume) was introduced. The NO_x species adsorption spectra

were collected at various target temperatures at a rate of 10 ^{o}C min^{-1} from room temperature to 300^{o}C by subtraction of the corresponding background reference.

Catalytic conversion of NO. The catalytic activity and selectivity of these catalysts were determined under light-off procedure in NO+CO model reaction, involving a feed steam with a fixed composition, 5% NO, 10% CO and 85% He by volume as diluents. The sample (25 mg) was pretreated in a high purified N_2 stream at 300 ^{o}C for 1 h and then cooled to room temperature, after that, the mixed gases were switched on. The reactions were carried out at different temperatures with a space velocity of 24,000 ml g^{-1}h^{-1}. Two columns (length, 1.75 m; diameter, 3 mm) and thermal conductivity detector (T=100 ^{o}C) were used for analyzing the products. Column A with Paropak Q for separating CO_2 and N_2O, column B packed with 5A and 13X molecule sieve (40–60 M) for separating N_2, NO and CO.

Theoretical calculations. All DFT calculations are performed using the VASP [13, 14] code with projected augmented wave (PAW [15]) method. Generalized gradient approximation (GGA[16]) in the scheme of Perdew-Bueke-Ernzerhof (PBE [17]) is used for the exchange correlation functional. The cutoff energy is 500 eV. The geometry relaxations are performed until the residual forces on each ion converged to be smaller than 0.01 eV/Å. Since the $NiGa_2O_4$ is an inverse spinel compound, it is firstly necessary to construct an atomic model for the DFT calculation. For the simplicity purpose, we adopt the primitive cell of the $NiGa_2O_4$. In the primitive cell, two Ni atoms are randomly distributed on the four lattice sites of one tetrahedron. Then, we construct six possible $NiGa_2O_4$ models to check which model is energetically favorable. Based on the most stable $NiGa_2O_4$ model, one Ni atom is further substituted by one Zn atom to construct the Zn-doped $NiGa_2O_4$. The concentrations of the Zn in this cell is 50%. To calculate the Bader charges before and after doping Zn into $NiGa_2O_4$, the $NiGa_2O_4$ (311) surface is simulated using a slab which consists of 27 O, 7 Ni and 14 Ga atoms. And the $NiGa_2O_4$ (111) surface is simulated using a slab which consists of 40 O, 11 Ni

and 22 Ga atoms. To avoid interaction between two surfaces of the slab, a vacuum thickness of 15 Å is added at each side of the slab. The 3×3×1 k-points meshes are adopted for this slab model. During relaxations, all atoms are allowed to relax. For simplicity purpose, the $NiGa_2O_4$ (311) surface with and without Zn doping are denoted as $NiGa_2O_4$-(311) and $NiGa_2O_4$+Zn_{Ni}-(311), respectively. The $NiGa_2O_4$ (111) surface with and without Zn doping are denoted as $NiGa_2O_4$-(111) and $NiGa_2O_4$+Zn_{Ni}-(111), respectively.

3. Results and Discussion

The $Ni_{1-x}Zn_xGa_2O_4$ ($0\leq x\leq 1$) catalyst was prepared by a hydrothermal ion exchange method based on a colloid reactive template[18]. In brief, introducing nickelous acetate and zinc acetate into the $NaGaO_2$ colloid solution, an ion exchange between Na^+ and Zn^{2+}/Ni^{2+} occurs during a hydrothermal reaction at 180 ^oC and the $Ni_{1-x}Zn_xGa_2O_4$ ($0\leq x\leq 1$) precipitate formed. The precipitate was filtered, washed and dried.

To evaluate catalytic performance, we exposed the as-prepared samples $Ni_{1-x}Zn_xGa_2O_4$ ($0\leq x\leq 1$) to the reactant gas mixture (5% NO, 10% CO and 85% He) while raising the temperature up to 550 ^oC to test for NO conversion. Fig. 1a and Table 1 demonstrate that the $NiGa_2O_4$ can be used as a catalyst for NO removal, exhibiting a beginning activity at ~250 ^oC and a maximum activity at 550 ^oC for complete conversion of NO into N_2 (Fig.1b). After Zn doping, the $Ni_{0.9}Zn_{0.1}Ga_2O_4$ offers improved NO conversion over the $NiGa_2O_4$ catalyst in the temperature range 250-550 ^oC. Further increasing the Zn content higher than Zn:Ni=1:9, the catalytic activity of the Ni-based catalysts decreased and the $ZnGa_2O_4$ displays the lowest activity. The generated N_2 from NO conversion was detected to be starting at 300 ^oC and showed the same variation tendency as NO removal at corresponding operating temperature, that is, for Ni-Ga based catalysts the conversion rate of NO to N_2 gradually increased with increasing the reaction temperature. It should be pointed out that the $Ni_{0.9}Zn_{0.1}Ga_2O_4$ exhibited higher performance in NO conversion to N_2 than 1wt% Pt loaded ZrO_2 catalyst at the temperature above 500 ^oC and the and good catalytic stability for recycling use (Fig.1c),

meaning that the Ni-Ga based oxide catalyst, which was synthesized by simple hydrothermal reaction using the cheap raw materials, is a promising low-cost catalyst for NO removal. In NO conversion, N_2O is a recognized intermediate product [6]. As shown in Fig.1d and Table 1, the N_2O was generated at the same temperature as conversion of NO to be starting at 250 ^oC. At the low temperature range (250-400 ^oC for $Ni_{0.9}Zn_{0.1}Ga_2O_4$ and $NiGa_2O_4$, 250-450 ^oC for $Ni_{0.5}Zn_{0.5}Ga_2O_4$ and $Ni_{0.1}Zn_{0.9}Ga_2O_4$), the catalytic activity in N_2O generation of the nickel containing catalysts increased with increasing reaction temperature. As the temperature further increases, the N_2O yield decreases and N_2 yield increases, indicating that the higher temperature can accelerate the N_2O intermediate product catalytically converting into N_2. However, for the $ZnGa_2O_4$, the N_2O yield continually increased with increasing the reaction temperatures.

The X-ray powder diffraction (XRD) pattern was obtained for characterizing the phase structure. As shown in Fig. 2a, the as-prepared $Ni_{1-x}Zn_xGa_2O_4$ can be well assigned to inverse spinel phase $NiGa_2O_4$ (x=0, JCPDS 10-0114) and the spinel phase $ZnGa_2O_4$ (x=1, JCPDS 38-1240). Increasing the Zn content in the $NiGa_2O_4$, the (311) diffraction peak gradually shifts to a lower diffraction angle because the ion radius of Zn^{2+} (0.074nm) is larger than that of Ni^{2+}(0.069 nm), indicating that the Zn^{2+} was incorporated into the crystal lattice of $NiGa_2O_4$. The transmission electron microscope (TEM) images in Fig. 2b and Fig.S1 in ESI reveal that the Ni-Ga based catalysts exhibited a porous structure, which was formed by the aggregation of nanocrystals with a particles size of 10-20 nm. A nitrogen adsorption-desorption measurement further confirmed that the $Ni_{1-x}Zn_xGa_2O_4$ is typical of mesoporous material with an average pore diameter about 7.0-8.0 nm and a specific surface area about 72.6-80.2 m^2g^{-1} (Fig. S2, ESI†). High crystallinity and the structural consistency were confirmed by scanning transmission electron microscope. The high-resolution lattice image shows that the (311) and (111) facets are the stable facets with high exposure percentage (Fig. 2c, 2d and Fig.S3, ESI†). To decrease the magnetism of as-prepared samples, the $Ni_{0.1}Zn_{0.9}Ga_2O_4$ with a low content of

the magnetic Ni was used for high-resolution TEM observations. High angle annular dark field (HAADF) image of a typical nanocrystal was clearly obtained, as shown in Fig.2e. The element mapping images shown in Fig.2e revealed that the Zn, Ni, Ga and O uniformly distributed in the as-prepared nanocrystals and X-ray photoelectron spectrum (XPS) demonstrated that the stoichiometry of the as-prepared $Ni_{1-x}Zn_xGa_2O_4$ product is close to the nominal element ratio. This evidence indicated that the Zn-doped $NiGa_2O_4$ was an uniform solid solution of $ZnGa_2O_4$ and $NiGa_2O_4$.

To understand the NO conversion reaction, we performed diffuse reflectance infrared Fourier transform spectroscopy (DRIFTS) on the as-prepared catalysts, $ZnGa_2O_4$, $Zn_{0.1}Ni_{0.9}Ga_2O_4$ and $NiGa_2O_4$. **Figure 3** depicts the evolution of NO_x species at different temperatures in 5%NO+10%CO+85%He gas environments. Bands at 1906 and 1864 cm^{-1} are observed in the all Ni containing catalysts, which can be respectively assigned to the N-O stretching frequencies of Ni^{2+}-NO species and the Ni^{2+}(CO)(NO) species[19]. The $ZnGa_2O_4$ without Ni ions did not exhibit the two bands, meaning that the NO or CO is indeed captured by the coordination of a NO or CO molecule to a Lewis acid (metal sites), Ni ions, via the nitrogen atom as well as carbon ato[20]. The bands observed in the 1100-1700 cm^{-1} region after NO adsorption can be attributed to nitrite/nitrate specie [20]. Bands located at 1550-1300 cm^{-1} were formed in all three samples, likely correspond to the NO_x species coordinating into the Ga species of catalyst surface. A band at 1549 cm^- can be assigned to bidentate Ga-nitrate and bands at 1498, 1455 and 1347 cm^- belong to monodentate Ga-nitrite. Noting that the $Ni_{0.9}Zn_{0.1}Ga_2O_4$ exhibited the significant increase in intensity of bidentate Ga-nitrate band at 1549 cm^- with increasing the reaction temperature, indicating that the adsorption of nitrate species on $NiGa_2O_4$ surface is largely improved by incorporation of Zn. The spectrum bands at 1305cm^- for $ZnGa_2O_4$ and 1312cm^- for $Ni_{0.9}Zn_{0.1}Ga_2O_4$ are in good agreement with the observations on adsorption of monodentate nitrate (NO_3^-) on Ga_2O_3[21] and Ni-containing zeolites[22], respectively. This indicates that the Ga in $ZnGa_2O_4$ as well as in Ga_2O_3 acts as the

active adsorption site for formation of NO_3^-, however, for $Ni_{0.9}Zn_{0.1}Ga_2O_4$, the Ni is. NO_x adspecies, probably NO_3^-, formed on the catalyst surface is known to play an important role in NO reduction[23]. Indeed, in our case, the surface monodentate nitrate concentration over $ZnGa_2O_4$ and $Ni_{0.9}Zn_{0.1}Ga_2O_4$ decreased with increasing the reaction temperature, implying that the nitrate species converted rapidly at high temperature.

After Zn doping into $NiGa_2O_4$, an obvious change is that a novel band at 1278cm$^-$ assignable to NO_3^- species occurred[24]. The NO_3^- species (1278cm$^-$) and the NO_2^- species (1498cm$^-$) respectively exhibited the increase and decrease intensity with raising the reaction temperature, meaning that the formation of NO_3^- resulted from the oxidation of NO_2^- [25]. Increasing the temperature higher than 50^{o}C, such a NO_3^- band also was observed in the $ZnGa_2O_4$ and exhibited the good high-temperature stability, probably meaning that the Ga-NO_3^- band resulted from the change of coordination environment of Ga atoms on catalyst surface inducing by the temperature raising for $ZnGa_2O_4$ as well as Zn doping for $NiGa_2O_4$. A direct evidence to show the effect of temperature on NO_x species over Ga-based catalysts is that a novel band at 1236 cm$^-$ in all three samples appeared at high temperature, which can be belonged to the monodentate Ga-nitrate [24].

The $N_{i0.1}Zn_{0.9}Ga_2O_4$ was used for decreasing magnetism of sample itself to perform the electron paramagnetic resonance analysis. The as-prepared $Ni_{0.1}Zn_{0.9}Ga_2O_4$ is light green in color, in accordance with the color of Ni^{2+}. Heating the sample at 300 ^{o}C, under 5% NO/Ar gas atmosphere, the sample turned into light yellow immediately. The EPR spectra for the $Ni_{0.1}Zn_{0.9}Ga_2O_4$ sample before and after heat treatment at 300 ^{o}C in NO were recorded at 77K and shown in Fig. 4. The $Ni_{0.1}Zn_{0.9}Ga_2O_4$ before heat treatment did not show any paramagnetic signal. After heat treatment in NO, the EPR spectrum revealed paramagnetic signals at *g* values of 2.20, 2.15, and 2.06, which are an indication of Ni^{3+} [26]. UV-Vis absorption spectra confirmed that the absorption edge of $Ni_{0.1}Zn_{0.9}Ga_2O_4$ are largely red-shifted after heat treatment in NO (Fig. S4a, ESI†). A density functional theory (DFT)

calculation indicated that when Ni^{2+} was oxidized to Ni^{3+}, the photoabsorption of the $Ni_{0.9}Zn_{0.1}Ga_2O_4$ extends to visible light region (Fig. S4b, ESI†). The change of the photoabsorption is in good agreement with the UV-Vis spectra, thus illustrates that the $Ni_{0.1}Zn_{0.9}Ga_2O_4$ exhibits different photoabsorption property with different nickel oxidation states. It has been demonstrated that oxygen converted Ni^{2+} to Ni^{3+}, which was kinetically and thermodynamically stabilized in the tetraglycine complexes [27]. In our case, the color change from light green to light yellow is more faster for heating the $Ni_{0.1}Zn_{0.9}Ga_2O_4$ in NO than in O_2, verifying that in the presence of NO oxidizing Ni^{2+} to Ni^{3+} occurs more easily. After heat treatment of $Ni_{0.1}Z_{0.9}nGa_2O_4$ in NO, an observed low-field paramagnetic signal at g=2.006 in EPR spectrum of Fig.4 corresponds to oxygen vacancies with a single trapped electron [28]. A DRIFTS band at 1628 cm^{-1} shown in Fig.3c is assigned to NO_2 vibration [29], which mainly originated from the NO oxidation[30, 31]. Considering the EPR and DRIFTS results, the oxygen vacancies formed in the Zn-doped $NiGa_2O_4$ during the NO conversion would be attributed to that active lattice oxygen on the catalyst surface takes part in the oxidation of NO into NO_2. The lattice oxygen converted NO into NO_2 and nitrate species has been observed in many catalysts such as the representative Ce-Zr-based materials [32]. Based on such a mechanism, an efficient NO removal route with reversible process of storing and releasing oxygen into/from crystal lattice of oxides was developed in order to enlarge the operating window near the stoichiometry to convert simultaneously NO_x, CO and unburned hydrocarbons.

It is important to understand the nature of high activity of Ni-Ga based materials. A significant difference is the different cation distribution in $NiGa_2O_4$ and $ZnGa_2O_4$. $NiGa_2O_4$, exhibiting the high activity in catalytic conversion of NO, belongs to a largely inverse spinel with an inversion parameter of 92%, the tetrahedral preference of Ga^{3+} and the octahedral preference of Ni^{2+}, due to the well-known crystal field stabilization effects [33]. However, $ZnGa_2O_4$ with the low activity for converting NO is a normal spinel, in which crystal the Zn^{2+} and Ga^{3+} located at tetrahedral and octahedral sites, respectively. The catalytic performance of

metal cations is dependent strongly on the ligand environments, which affect the electron transfer and stability of cations. It has been demonstrated that the different ligand environments of Ga will induce the large difference in catalytic activity of the gallium oxide catalysts [34]. For instance, the β-Ga_2O_3, which is composed of both tetrahedral and octahedral Ga ions in a spinel phase, shows 20 times higher activity in NO conversion than α-Ga_2O_3, containing only octahedral Ga ions. Using the Al_2O_3 as a support, the Ga_2O_3 shows a higher NO conversion due to the formation of Ga-O-Al species which controls the local structure of Ga species and provides stabilization of Ga ions in the low coordination environment, resulting in a high performance for NO conversion. Similarly, in our case, compared to the $ZnGa_2O_4$ with octahedral Ga^{3+} species, the high activity of $NiGa_2O_4$ would originate from the tetrahedral preference of Ga^{3+} species.

Element doping is an efficient method to improve the ligand environment of the cations for decreasing the excess potential for electron transfer. After Zn doping, the NO catalytic conversion on $NiGa_2O_4$ was significantly improved. The Zn^{2+} is expected to replace the Ni^{2+} sites of $NiGa_2O_4$ due to the small difference in ion radius (Zn^{2+}, 0.074nm; octahedral Ni^{2+}, 0.069nm) [33]. Bader charge based on DFT calculations is a powerful tool to reflect the electron gain and loss of ions [35]. (311) and (111) surface models of Zn-doped $NiGa_2O_4$ were constructed to calculate the Bader charge because TEM observations reveal that the $NiGa_2O_4$ (311) and (111) facets were relatively more stable (Fig.S3, ESI†). For simplicity purpose, the $NiGa_2O_4$ (311) and (111) surfaces with and without Zn doping are denoted as $NiGa_2O_4$+Zn_{Ni}-(311), $NiGa_2O_4$-(311) and $NiGa_2O_4$+Zn_{Ni}-(111), $NiGa_2O_4$-(111), respectively**.** Fig. 5 shows the calculated Bader charges for $NiGa_2O_4$ (311) and (111) surfaces with and without Zn doping. As is well-known, for the metal ions, the more positive Bader charge indicates that more electrons are lost. The Bader charges of all Ga ions on $NiGa_2O_4$-(311) and $NiGa_2O_4$-(111) surfaces are more positive than those on $NiGa_2O_4$+Zn_{Ni}-(311) and $NiGa_2O_4$+Zn_{Ni}-(111) surfaces, suggesting that less electrons are lost from the Ga ions after Zn doping into $NiGa_2O_4$

(311) and (111) surfaces. This means that, during the adsorption reactions, the Ga ions on the $NiGa_2O_4$+Zn_{Ni}-(311) surface are able to donate more electrons to the ad-species such as nitrate and nitrite. In-situ XPS analysis was carried out to check the electron transfer in the $Ni_{0.9}Zn_{0.1}Ga_2O_4$. The XPS spectra were obtained at room temperature in vacuum (denoted as $Ni_{0.9}Zn_{0.1}Ga_2O_4$-RT) and after heating at 400^{o}C in NO atmosphere (denoted as $Ni_{0.9}Zn_{0.1}Ga_2O_4$-400), respectively, as shown in Fig.S5 in ESI. Compared to $Ni_{0.9}Zn_{0.1}Ga_2O_4$-RT, the binding energy of the cations Ga 3d, Ni 2p and Zn 2p of $Ni_{0.9}Zn_{0.1}Ga_2O_4$-400 exhibited a positive chemical shift about 0.18 eV, 0.27eV and 0.2eV, respectively. O1s spectra did not present the obvious change in binding energy for $Ni_{0.9}Zn_{0.1}Ga_2O_4$ before and after heating, probably due to the oxygen vacancies were high activity in oxygen capture from the NO_x species at as high temperature as 400^{o}C. The increase in binding energy of cations means that the electrons are partly lost, that is, the electron transfer process occurs during heating $Ni_{0.9}Zn_{0.1}Ga_2O_4$ in NO atmosphere. This also indicated that there is an interaction between the NO_x species and cations, which induced the electron transfer process to occur. Indeed, the chemical shift of binding energy of Zn ions confirmed that the Zn ions can take part in the electron transfer process, thus promoting the catalytic ability of $NiGa_2O_4$.

EPR spectra indicated that Zn doping into $NiGa_2O_4$ will induce formation of the oxygen vacancies in the presence of NO (Fig.4). It is widely reported that surface oxygen vacancy is beneficial to the dissociation of NO species [36-38], obviously promoting the NO conversion. In addition, the DRIFTS spectra presented that the Ni species possesses a strong ability to capture NO and CO and EPR spectra revealed that a Ni^{2+}/Ni^{3+} catalytic redox couple formed during the NO conversion. The strong gas capture from Ni species and the formation of Ni^{2+}/Ni^{3+} catalytic redox couple would contribute to the high catalytic activity of Ni-Ga based materials. The formation of Ni^{2+}/Ni^{3+} catalytic redox couple depends on the NO atmosphere and Zn doping. As demonstrated by UV-Vis spectra (not shown here) that, compared to $NiGa_2O_4$, the Ni^{3+} species occurs more easily in the $Ni_{0.9}Zn_{0.1}Ga_2O_4$ in the presence of NO at as low temperature as 200^{o}C due to the formation of NO_x species from NO oxidation, which are strong electron acceptor. Indeed, the $Ni_{0.9}Zn_{0.1}Ga_2O_4$ is stable below 300^{o}C in the air, meaning that molecular oxygen is not able to oxidize the Ni^{2+} into Ni^{3+} under that

temperature. Moreover, it seems possible that introducing Zn into $NiGa_2O_4$, a charge equilibrium of $Ni^{2+}+Zn^{2+}\rightarrow Ni^{3+}+Zn^{1+}$ can stabilize the Ni^{3+} species, which promotes the formation of Ni^{2+}/Ni^{3+} catalytic redox couple and contributes to the high catalytic activity of $Ni_{0.9}Zn_{0.1}Ga_2O_4$.

An additional experiment was carried out to demonstrate that the nitrates and nitrites are the important species for reduction of NO to N_2. Heating the $NaNO_3$ or $NaNO_2$ aqueous solution containing $Ni_{0.9}Zn_{0.1}Ga_2O_4$ at 80°C for 10h, the nitrates and nitrites are separately adsorbed on the $Ni_{0.9}Zn_{0.1}Ga_2O_4$ catalyst surface. We found that converting Ni^{2+} to Ni^{3+} on both the nitrates and nitrites adsorbed catalyst surfaces shows the nearly same starting temperature and is in reasonably good agreement with the catalysts' operating temperature to be about 250°C. This indicates that the adsorbed nitrites and nitrates appeared to be true and important intermediates in NO conversion, which are more stable decomposing in the range of 200-600°C [39]. Therefore, it seems a reasonable deduction that the NO molecules were captured on the Ni sites and then oxidized to NO_2 by lattice oxygen. Subsequently, nitrates and nitrites were catalytically formed on both Ga and Ni sites because the NO_x species were easily activated between two adjacent Ga and Ni sites by co-adsorption. The nitrates and nitrites decomposed and were reduced by CO to N_2.

4. Conclusions

In summary, we showed that inverse spinel-phase Zn-modified $NiGa_2O_4$ can catalytically convert the NO into N_2. In such Ni-Ga based catalyst, we achieved combining the gas trap sites and catalytic active sites into a single compound: as shown in Fig.5e, the Ni element exhibited significantly strong ability in capturing NO and the Ga element presented the strong catalytic ability in NO_x conversion. A low coordination Ga in the inverse spinel structure significantly contributed to the high activity of Ni-Ga based catalysts due to the easy electron transfer. Incorporating the Zn element into the Ni-Ga based catalyst, the synergetic catalysis of Ni and Ga is further enhanced due to the increased electron transfer between metal ions. Our finding opens the novel strategy to design the low-cost catalyst combining the robust NO_x gas capture sites and catalytic conversion sites in a single compound catalyst.

Acknowledgments

This work is supported by the National Basic Research Program of China (973 Program, 2013CB632404) and the National Natural Science Foundation of China (Nos. 51102132, 11174129, 51272101, and 51272102)..

Reference

1. M. Shelef, *Chemical Reviews*, 1995, **95**, 209-225.
2. S. Roy and A. Baiker, *Chemical Reviews*, 2009, **109**, 4054-4091.
3. P. Granger and V. I. Parvulescu, *Chemical Reviews*, 2011, **111**, 3155-3207.
4. E. Roedel, A. Urakawa, S. Kureti and A. Baiker, *Physical Chemistry Chemical Physics*, 2008, **10**, 6190-6198.
5. T. Lesage, J. Saussey, S. Malo, M. Hervieu, C. Hedouin, G. Blanchard and M. Daturi, *Applied Catalysis B:Environmental*, 2007, **72**, 166-177.
6. I. V. Yentekakis, R. M. Lambert, M. S. Tikhov, M. Konsolakis and V. Kiousis, *Journal of Catalysis*, 1998, **176**, 82-92.
7. W. S. Epling, L. E. Campbell, A. Yezerets, N. W. Currier and J. E. Parks, *Catalysis Reviews-Science and Engineering*, 2004, **46**, 163-245.
8. H. Abdulhamid, E. Fridell and M. Skoglundh, *Applied Catalysis B-Environmental*, 2006, **62**, 319-328.
9. J. G. Kim, H. M. Lee, M. J. Lee, J. H. Lee, J. G. Kim, J. Y. Jeon, S. K. Jeong, S. J. Yoo and S. S. Kim, *Journal of Industrial and Engineering Chemistry*, 2008, **14**, 841-846.
10. U. G. Alkemade and B. Schumann, *Solid State Ionics*, 2006, **177**, 2291-2296.
11. G. Busca, L. Lietti, G. Ramis and F. Berti, *Applied Catalysis B:Environmental*, 1998, **18**, 1-36.
12. N. Bogdanchikova, F.C. Meunier,M. Avalos-Borja, J.P. Breen, A. Pestryakov. Applied Catalysis B: Environmental, 2002, 36, 287 – 297.
13. G. Kresse and J. Hafner, *Phys Rev B*, 1993, **47**, 558-561.
14. G. Kresse and J. Furthmuller, *Computational Materials Science*, 1996, **6**, 15-50.
15. P. E. Blochl, *Phys Rev B*, 1994, **50**, 17953-17979.
16. J. P. Perdew, J. A. Chevary, S. H. Vosko, K. A. Jackson, M. R. Pederson, D. J. Singh and C. Fiolhais, *Phys Rev B*, 1992, **46**, 6671-6687.
17. J. P. Perdew, K. Burke and M. Ernzerhof, *Physical Review Letters*, 1996, **77**, 3865-3868.
18. S. C. Yan, S. X. Ouyang, J. Gao, M. Yang, J. Y. Feng, X. X. Fan, L. J. Wan, Z. S. Li, J. H. Ye, Y. Zhou and Z. G. Zou, *Angewandte Chemie-International Edition*, 2010, **49**, 6400-6404.
19. M. Mihaylov and K. Hadjiivanov, *Langmuir*, 2002, **18**, 4376-4383.
20. K. I. Hadjiivanov, *Catalysis Reviews-Science and Engineering*, 2000, **42**, 71-144.
21. M. Haneda, E. Joubert, J. C. Menezo, D. Duprez, J. Barbier, N. Bion, M. Daturi, J. Saussey, J. C. Lavalley and H. Hamada, *Journal of Molecular Catalysis a-Chemical*, 2001, **175**, 179-188.
22. M. Mihaylov, K. Hadjiivanov and D. Panayotov, *Applied Catalysis B-Environmental*, 2004, **51**, 33-42.
23. S. Kameoka, Y. Ukisu and T. Miyadera, *Physical Chemistry Chemical Physics*, 2000, **2**, 367-372.

24. M. Haneda, Y. Kintaichi, T. Mizushima, N. Kakuta and H. Hamada, *Applied Catalysis B-Environmental*, 2001, **31**, 81-92.
25. C. Drouet, P. Alphonse and A. Rousset, *Physical Chemistry Chemical Physics*, 2001, **3**, 3826-3830.
26. S. Foerster, M. Stein, M. Brecht, H. Ogata, Y. Higuchi and W. Lubitz, *Journal of the American Chemical Society*, 2003, **125**, 83-93.
27. F. P. Bossu, E. B. Paniago, D. W. Margerum, S. T. Kirksey and J. L. Kurtz, *Inorganic Chemistry*, 1978, **17**, 1034-1042.
28. V. Ischenko, S. Polarz, D. Grote, V. Stavarache, K. Fink and M. Driess, *Advanced Functional Materials*, 2005, **15**, 1945-1954.
29. N. Tang, Y. Liu, H. Q. Wang and Z. B. Wu, *Journal of Physical Chemistry C*, 2011, **115**, 8214-8220.
30. C. Yokoyama and M. Misono, *Journal of Catalysis*, 1994, **150**, 9-17.
31. L. Olsson, H. Sjovall and R. J. Blint, *Applied Catalysis B-Environmental*, 2009, **87**, 200-210.
32. M. W. Zhao, M. Q. Shen and J. Wang, *Journal of Catalysis*, 2007, **248**, 258-267.
33. C. O. Arean and M. C. Trobajofernandez, *Physica Status Solidi a-Applied Research*, 1985, **92**, 443-447.
34. K. Shimizu, A. Satsuma and T. Hattori, *Catalysis Surveys from Japan*, 2000, **4**, 115-123.
35. R. F. W. Bader, *Chemical Reviews*, 1991, **91**, 893-928.
36. B. Wen and M. Y. He, *Applied Catalysis B-Environmental*, 2002, **37**, 75-82.
37. J. F. Chen, Y. Y. Zhan, J. J. Zhu, C. Q. Chen, X. Y. Lin and Q. Zheng, *Applied Catalysis a-General*, 2010, **377**, 121-127.
38. L. J. Liu, Z. J. Yao, Y. Deng, F. Gao, B. Liu and L. Dong, *Chemcatchem*, 2011, **3**, 978-989.
39. V. A. Sadykov, S. L. Baron, V. A. Matyshak, G. M. Alikina, R. V. Bunina, A. Y. Rozovskii, V. V. Lunin, E. V. Lunina, A. N. Kharlanov, A. S. Ivanova and S. A. Veniaminov, *Catalysis Letters*, 1996, **37**, 157-162.

Table 1 Catalytic activity and selection for NO conversion over various catalysts at 550°C

Samples	Activity in NO conversion (%)	Selection	
		N_2O (%)	N_2 (%)
$ZnGa_2O_4$	21.7	16.3	5.3
$Zn_{0.1}Ni_{0.9}Ga_2O_4$	100	0	99.9
$Zn_{0.5}Ni_{0.5}Ga_2O_4$	67.1	0	66.8
$Zn_{0.9}Ni_{0.1}Ga_2O_4$	73.3	1.1	72.2
$NiGa_2O_4$	100	0	99.9

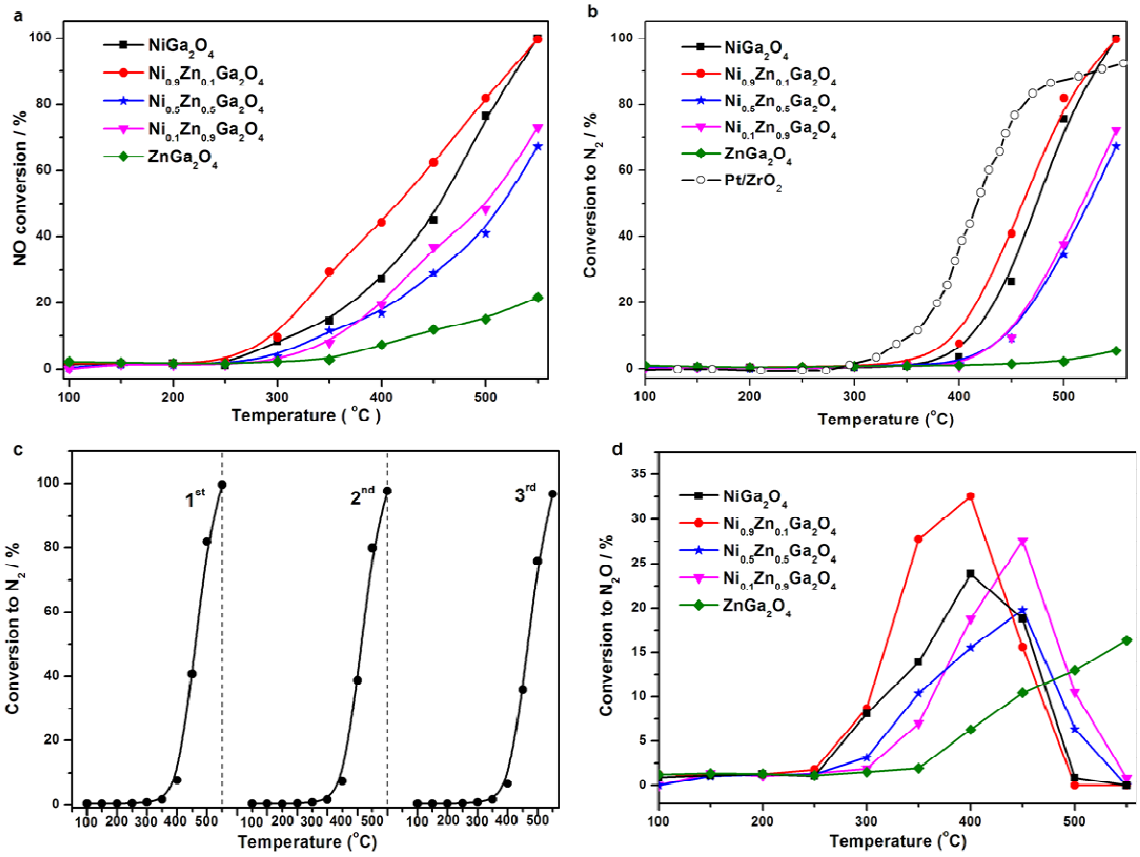

Figure 1 NO_x conversion versus ramp-up temperatures for various catalysts. (**a**) Total NO conversion. (**b**) NO conversion to N_2. (**c**) Three cycling stability test for NO conversion to N_2 over $Ni_{0.9}Zn_{0.1}Ga_2O_4$ catalyst.(**d**) NO conversion to N_2O.

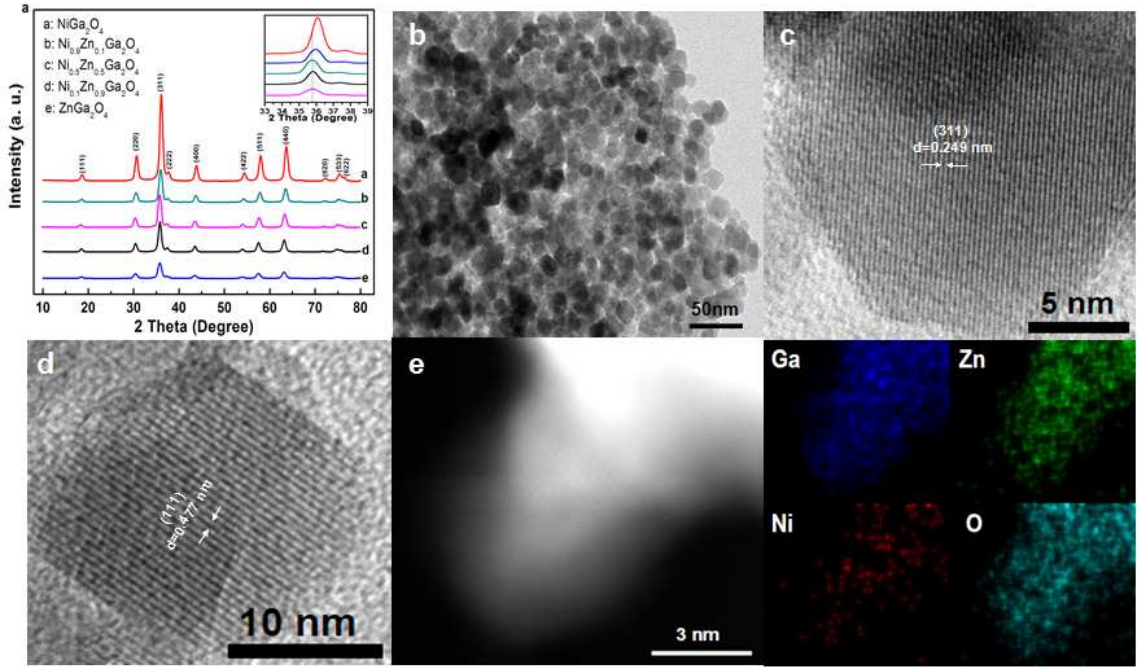

Figure 2 Structural properties for the as-prepared $Ni_{1-x}Zn_xGa_2O_4$ ($0 \leq x \leq 1$) . (**a**) XRD patterns. Inset shows (311) diffraction peak for various samples. (**b**) TEM image for $Ni_{0.9}Zn_{0.1}Ga_2O_4$. (**c**) High-resolution lattice image of $Ni_{0.9}Zn_{0.1}Ga_2O_4$ for (311) facet. (**d**) High-resolution lattice image of $Ni_{0.9}Zn_{0.1}Ga_2O_4$ for (111) facet. (**e**) HAADF image of $Ni_{0.1}Zn_{0.9}Ga_2O_4$ and corresponding Ga, Zn, Ni and O elements mapping.

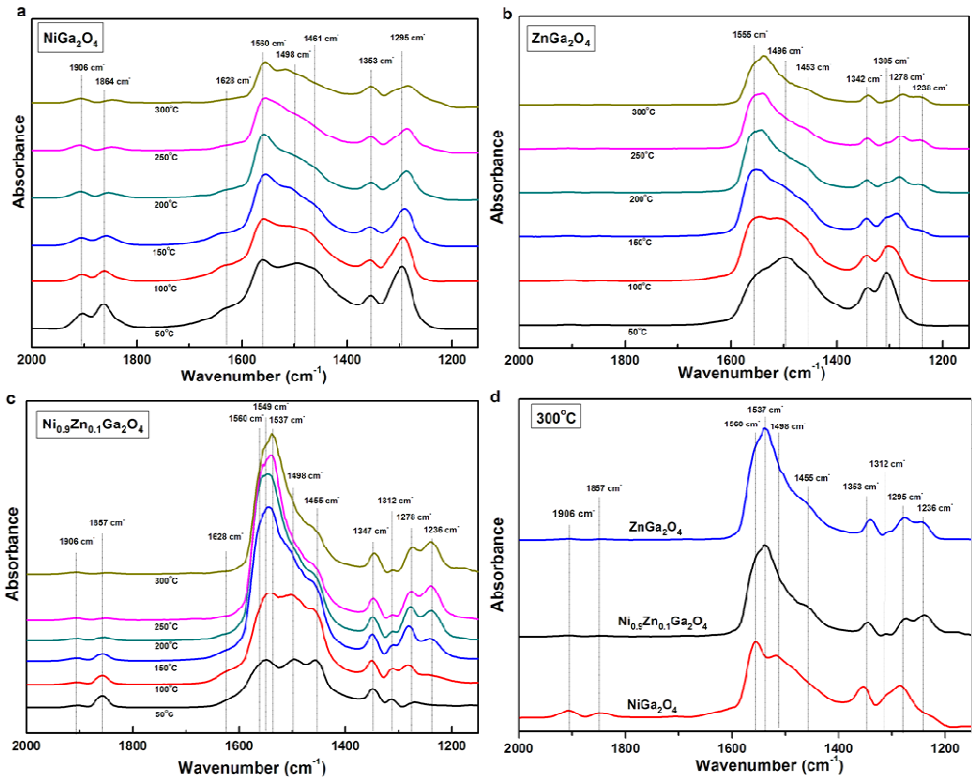

Figure 3 Evolution of DRIFTS spectra on as-prepared catalysts during exposure to NO+CO feed gases with temperatures. (**a**) $NiGa_2O_4$. (**b**) $Ni_{0.9}Zn_{0.1}Ga_2O_4$. (**c**) $ZnGa_2O_4$. (d) The DRIFTS spectra for various samples at 300°C.

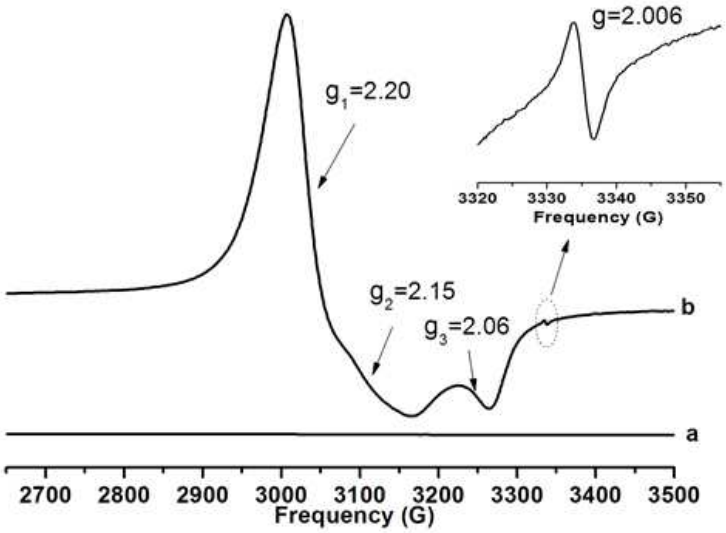

Figure 4 EPR spectra for the $Ni_{0.1}Zn_{0.9}Ga_2O_4$ catalyst. Curve a: Catalyst without heat treatment. Curve b: Catalyst after heating at 300°C under NO atmosphere. Inset shows the EPR signal in the frequency range from 3320 to 3350G.

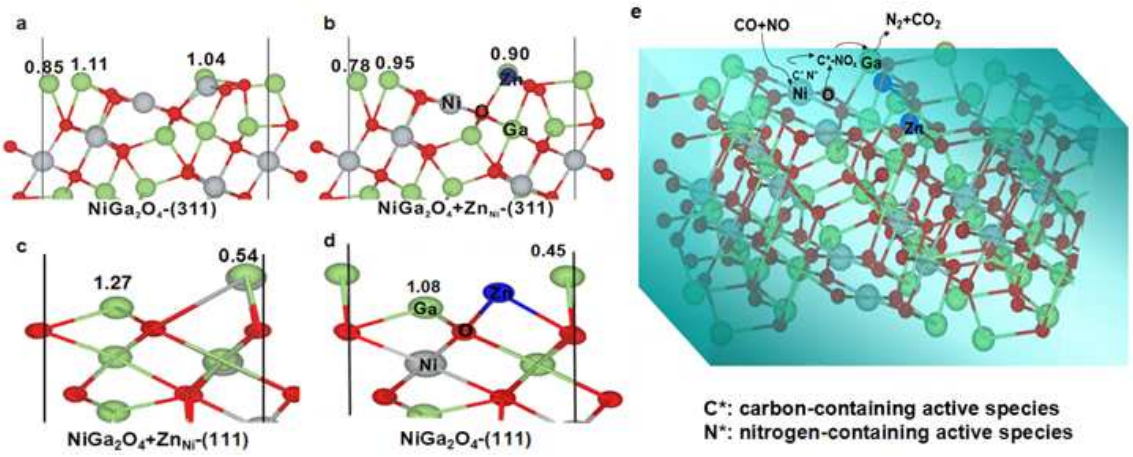

Figure 5 Calculated Bader charges for Ga ions and proposed NO_x conversion mechanism. (**a**) $NiGa_2O_4$-(311) facet. (**b**) $NiGa_2O_4+Zn_{Ni}$-(311) facet. (**c**) $NiGa_2O_4$-(111) facet. (**d**) $NiGa_2O_4+Zn_{Ni}$-(111) facet. (**e**) NO_x conversion over Ni-Ga based catalyst.